Article

Dexterous magnetic manipulation of conductive non-magnetic objects

Lan N. Pham[1], Griffin F. Tabor[2], Ashkan Pourkand[2], Jacob L. B. Aman[3], Tucker Hermans[2,4] & Jake J. Abbott[1✉]

Dexterous magnetic manipulation of ferromagnetic objects is well established, with three to six degrees of freedom possible depending on object geometry[1]. There are objects for which non-contact dexterous manipulation is desirable that do not contain an appreciable amount of ferromagnetic material but do contain electrically conductive material. Time-varying magnetic fields generate eddy currents in conductive materials[2–4], with resulting forces and torques due to the interaction of the eddy currents with the magnetic field. This phenomenon has previously been used to induce drag to reduce the motion of objects as they pass through a static field[5–8], or to apply force on an object in a single direction using a dynamic field[9–11], but has not been used to perform the type of dexterous manipulation of conductive objects that has been demonstrated with ferromagnetic objects. Here we show that manipulation, with six degrees of freedom, of conductive objects is possible by using multiple rotating magnetic dipole fields. Using dimensional analysis[12], combined with multiphysics numerical simulations and experimental verification, we characterize the forces and torques generated on a conductive sphere in a rotating magnetic dipole field. With the resulting model, we perform dexterous manipulation in simulations and physical experiments.

Magnetic manipulation has the benefit of being contactless, which is particularly attractive when there is a risk of destructive collision between the manipulator and target. Such is the case with space debris[13,14], a considerable problem facing humanity owing to the Kessler syndrome[15]. Most artificial space objects are fabricated primarily from aluminium[16], a non-magnetic but conductive material on which forces and torques can be generated by inducing eddy currents. The most commonly proposed application of this phenomenon is detumbling satellites by applying a static magnetic field to a rotating target. There exist numerical solutions for induced forces and/or torques on spinning solid and thin-walled spheres in uniform and non-uniform magnetic fields[5–7]. An alternative method of detumbling satellites uses rotating Halbach arrays near the target[10]. Rotating Halbach arrays have also been proposed as a means of traversing the exterior of the International Space Station (modelled as an infinite flat plate) using forces induced by eddy currents[9]. This technique is similar to that used in eddy-current separation of non-magnetic materials[11]. Methods based on eddy currents are distinct from those based on diamagnetism[17] or ferrofluid environments[18], neither of which are applicable to manipulation of objects at a distance.

Here we show that dexterous manipulation of conductive objects is achievable using multiple static (in position) magnetic dipole-field sources capable of continuous dipole rotation about arbitrary axes. We demonstrate manipulation with six degrees of freedom (6-DOF manipulation) in numerical microgravity simulations and 3-DOF manipulation in experimental microgravity simulations. This manipulation does not rely on dynamic motion of the conductive object itself; rather, the manipulation can be performed quasistatically. Both electromagnet and permanent-magnet devices have been developed to serve as field sources capable of generating continuously rotating magnetic dipole fields about arbitrary axes[19,20]. Rotating magnetic dipole fields have been used previously to remotely actuate ferromagnetic devices that transduce the resulting magnetic torque into some form of rotational motion, such as micromachines and magnetic capsule endoscopes[1].

To make our problem tractable, we explicitly consider conductive spheres, which can serve as first-order approximations for other geometries. Furthermore, we characterize those spheres in three canonical positions relative to a rotating magnetic dipole, as depicted in Fig. 1. Using cylindrical coordinates, the z-axis aligns with the angular-velocity vector $\boldsymbol{\omega}$ of the rotating dipole, with the dipole always orthogonal to that vector. We consider positions in the $\pm z$ axial directions and the radial direction ρ. When using a magnetic dipole-field source capable of dipole rotation about arbitrary axes, any given position can be transformed into each of these canonical positions through the choice of the dipole rotation axis. The magnetic dipole can be abstracted as a point dipole $\mathbf{m}$ (units A m^2) at position $\mathcal{P}_{\mathbf{m}}$, which generates a magnetic field vector $\mathbf{b}$ (units T) at each position $\mathcal{P}_{\mathbf{b}}$ in space:

$$\mathbf{b} = \frac{\mu_0}{4\pi\|\mathbf{d}\|^3}\left(\frac{3\mathbf{d}\mathbf{d}^{\mathsf{T}}}{\|\mathbf{d}\|^2} - I\right)\mathbf{m} \tag{1}$$

[1]Department of Mechanical Engineering, University of Utah, Salt Lake City, UT, USA. [2]School of Computing, University of Utah, Salt Lake City, UT, USA. [3]Lawrence Livermore National Laboratory, Livermore, CA, USA. [4]NVIDIA, Seattle, WA, USA. ✉e-mail: jake.abbott@utah.edu
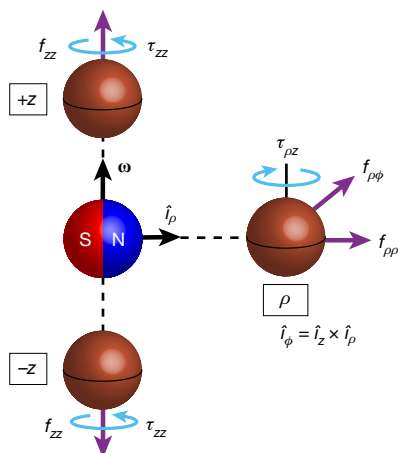
Article

Fig. 1 | Induced forces and torques on a conductive sphere in three canonical positions relative to a rotating magnetic dipole. The dipole is spinning with angular velocity $\boldsymbol{\omega}$. Force and torque arrows are shown for all non-negligible components, with arrowheads depicting the actual directions corresponding to the $\boldsymbol{\omega}$ shown.

where $\mathbf{d} = \mathcal{P}_\mathbf{b} - \mathcal{P}_\mathbf{m}$ is the relative displacement vector (units m), I is the identity matrix, $\mu_0 = 4\pi \times 10^{-7}$ N A^{-2} is the permeability of free space, and all vectors are expressed in a common frame of reference[1].

We begin by characterizing the steady-state time-averaged forces and torques, in each of the canonical positions, as a function of the six independent variables enumerated in Table 1. These quantities collectively comprise four dimensions: N, m, s and A. The Buckingham Π theorem tells us that the underlying physics describing each of the two dependent variables, force and torque, can be characterized using just three dimensionless Π groups[12], with Π_0 expressed as a function of Π_1 and Π_2 (see Table 1 and Supplementary Information 1). The Buckingham Π theorem does not tell us anything about the form of these equations; that requires empirical characterization.

To derive functions that characterize eddy-current-induced forces and torques at $\pm z$ and ρ, we conducted electromagnetic finite-element-analysis (FEA) simulations using Ansys Maxwell software across a range of parameters (see Fig. 2a and Supplementary Information 2). It is from this FEA that we determined the non-negligible force and torque components shown in Fig. 1. We confirmed the expected symmetry of the $\pm z$ configurations, in which the force acts to push the sphere away from the rotating dipole, and the torque acts to rotate the sphere in the same direction as $\boldsymbol{\omega}$. At the ρ configuration, one component of the force pushes the sphere away from the rotating dipole, another component of the force pushes the sphere in the $\hat{i}_\phi = \hat{i}_z \times \hat{i}_\rho$ direction, and the torque acts to rotate the sphere opposite to $\boldsymbol{\omega}$.

When visualizing the resulting non-dimensional Π groups (see Fig. 2b and Supplementary Information 3), we observed that at relatively far distances ($\Pi_2 > 1.5$, approximately), the relationship between $\log_{10}(\Pi_0)$ and $\log_{10}(\Pi_2)$, for a given Π_1, is accurately described by a linear model, with a slope of −6 for torques and −7 for forces (these values are analogous to what is expected from magnetic torques and forces imparted by a magnetic dipole on a soft-magnetic object), and with an intercept that is a function of Π_1. The final unified model is of the form

$$\Pi_0 = \frac{(c_0 \Pi_1)^{c_1 \Pi_1{}^{c_2}} 10^{c_3}}{\Pi_2{}^{c_4}} \qquad (2)$$

The model coefficients c_1 to c_4, determined through least-squares regression, are provided for 'FEA' in Supplementary Table 2

of Supplementary Information 3. This model, although empirically determined, is well behaved in the sense that $\Pi_0 \to 0$ (that is, $f \to 0$ or $\tau \to 0$) as $\Pi_1 \to 0$ (for example, as $\omega \to 0$ or $\sigma \to 0$) or as $\Pi_2 \to \infty$ (for example, as $d \to \infty$), as expected from first principles. At relatively close distances, this model underpredicts the data, making the model conservative.

Next, we experimentally verified the model described above with an experimental set-up comprising a cubic NdFeB permanent magnet rotated by a direct-current (d.c.) motor, a solid copper sphere mounted on a 6-DOF force-torque sensor, and a 3D-printed pegboard that enables the copper sphere to be placed in the three configurations of interest (see Fig. 2c and Supplementary Information 4). A sample of the resulting data with regression models is presented in Fig. 2d. Using the complete experimental data set, we fit the model of equation 2, with the resulting coefficients provided under 'Experiments' in Supplementary Table 2 of Supplementary Information 3.

As we compare the experimental and FEA results across configurations and force-torque components, we find good agreement in the overall trends. The FEA-based model tends to overpredict the experimental values of Π_0 by a factor of 1.5–5.5. This discrepancy could be due to impurities in the copper sphere or from using a cubic permanent magnet. However, field distortions from a cubic magnet relative to a point-dipole model are typically less than 5% in our region of implementation[21]. It has also been previously noted that Ansys Maxwell tends to overpredict experimental results in similar situations[10]. Considering these factors, we suggest using the experiment-based model as a lower bound and the FEA-based model as an upper bound for Π_0. Extrapolating the model beyond the values of Π_1 and Π_2 considered should be done with caution.

We now describe a framework for using the force-torque model developed above to perform dexterous manipulation with magnetic-dipole sources surrounding the conductive object of interest. This can take the form of stationary or mobile permanent magnets or electromagnets. Here, we focus exclusively on the case of stationary electromagnets, in which both m and $\boldsymbol{\omega}$ can be controlled, but with their respective maximum values coupled due to the low-pass-filtering effect of induction. We treat m and the direction of $\boldsymbol{\omega}$ as the control variables and simply use a constant angular-velocity magnitude ω. We assume n electromagnetic dipole-field sources, with the ith source located at position $\mathcal{P}_{ei}$ and having an orientation described by a rotation matrix $^{w}R_{ei}$ with respect to some world frame[22]. We assume a single conductive object located at position $\mathcal{P}_c$ and having an orientation described by $^{w}R_c$ and a displacement vector $\mathbf{d}_i = \mathcal{P}_c - \mathcal{P}_{ei}$ with respect to each source.

To use the model in equation 2, we recast forces and torques in the forms $f = \Pi_0 r^{-4} \mu_0 m^2$ and $\tau = \Pi_0 r^{-3} \mu_0 m^2$, respectively. Each source is given a model frame, described by a relative rotation matrix $^{ei}R_{mi}$, defined such that its z-axis is parallel to $\mathbf{d}_i$. In the $\pm z$ configurations, $\boldsymbol{\omega}$ is parallel or antiparallel to the model-frame z-axis, and in the ρ configuration $\boldsymbol{\omega}$ is any vector orthogonal to the z-axis, with the

Table 1 | Induced force and torque, and the six independent parameters that affect them

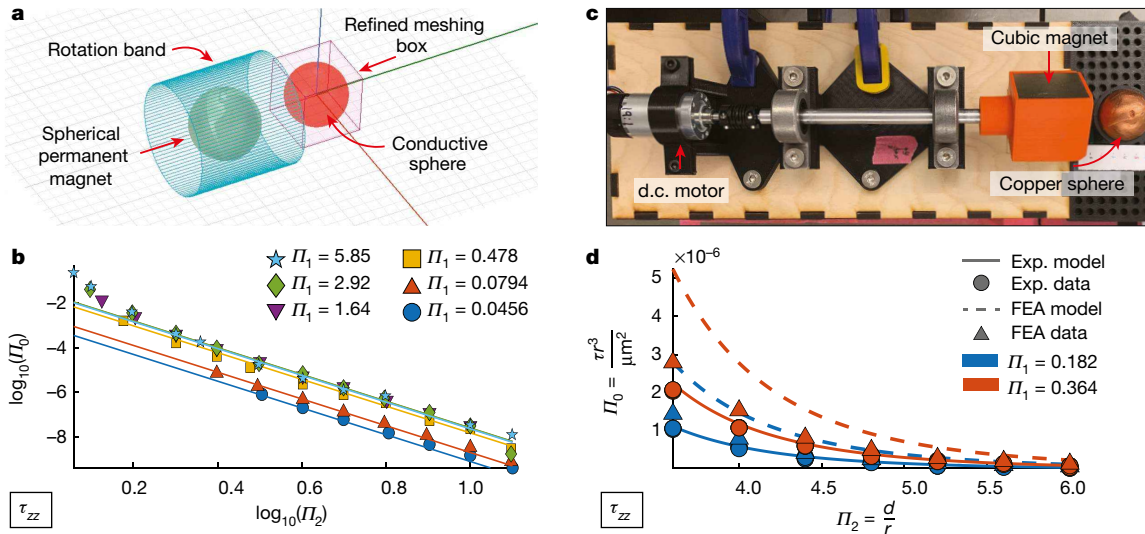| Parameter		Units	Π group
Force induced on sphere	f	N	$\Pi_0 = f r^4 \mu^{-1} m^{-2}$
Torque induced on sphere	τ	N m	$\Pi_0 = \tau r^3 \mu^{-1} m^{-2}$
Sphere electrical conductivity	σ	N^{-1} m^{-2} s A^2	$\Pi_1 = \sigma \mu \omega r^2$
Distance from dipole to sphere	d	m	$\Pi_2 = d r^{-1}$
Sphere radius	r	m	
Dipole strength	m	A m^2	
Frequency of dipole rotation	ω	s^{-1} (Hz)	
Environment magnetic permeability	μ	N A^{-2}	

Fig. 2 | Typical numerical and experimental results for force-torque characterization. For clarity, only a subset of the data for a single component τ_{zz} is shown. **a**, Rendering of FEA simulation. **b**, FEA data with unified regression model. **c**, Top view of experimental set-up. **d**, Experimental data with unified regression model. Unified FEA regression model with new FEA data not included in the training set.

ambiguity expressed as a rotation about the z-axis by some γ using a rotation matrix $\mathrm{Rot}_z(\gamma)$. Each source then has three discrete actions ($a \in \{1, 2, 3\}$, respectively) that can be performed on the conductive object, where each action is a specific force-torque wrench with a controllable magnitude:

$$
\begin{bmatrix} {}^w f \\ {}^w \tau \end{bmatrix} \in m^2 \begin{bmatrix} {}^w R_{mi} & 0 \\ 0 & {}^w R_{mi} \end{bmatrix} \left\{ \begin{bmatrix} 0 \\ 0 \\ \widetilde{f}_{zzi} \\ 0 \\ 0 \\ \widetilde{\tau}_{zzi} \end{bmatrix}, \begin{bmatrix} 0 \\ 0 \\ \widetilde{f}_{zzi} \\ 0 \\ 0 \\ -\widetilde{\tau}_{zzi} \end{bmatrix}, \begin{bmatrix} \mathrm{Rot}_z(\gamma) & 0 \\ 0 & \mathrm{Rot}_z(\gamma) \end{bmatrix} \begin{bmatrix} 0 \\ -\widetilde{f}_{\rho\phi i} \\ \widetilde{f}_{\rho\rho i} \\ -\widetilde{\tau}_{\rho z i} \\ 0 \\ 0 \end{bmatrix} \right\} \quad (3)
$$

where ${}^w R_{mi} = {}^w R_{ei}\,{}^{ei}R_{mi}$ and the tilde operator (~) indicates the respective force-torque value when $m = 1$.

With n sources, there are $3n$ possible actions, with m and γ as the control variables in general. Analogous to magnetic manipulation of soft-magnetic objects, superposition does not apply here, so we implement these actions one at a time, for a brief duration of time. To get as close as possible to the desired wrench, we solve the following constrained optimization problem:

$$
\underset{i,a,m,\gamma}{\arg\min} \left\| \begin{bmatrix} {}^w f_{\mathrm{des}} \\ {}^w \tau_{\mathrm{des}} \end{bmatrix} - \begin{bmatrix} {}^w f \\ {}^w \tau \end{bmatrix} \right\|_Q^2
$$

subject to
$$
i \in \{1, \cdots, n\}, \quad a \in \{1, 2, 3\}, \quad m \in [0, m_{\max}],
$$
$$
\gamma \in [-\pi, \pi]
$$
(4)

where the Q-norm enables relative weighting between force and torque (that is, relative penalties on position error versus orientation error). We efficiently find the optimal inputs using a parallelized, gradient-based solver.

We first validated our manipulation framework in a numerical simulation of microgravity in which six dipole-field sources surround and dexterously manipulate a copper sphere (see Supplementary

Information 6). We performed 3-DOF position control, with and without 3-DOF orientation control (see Fig. 3a–d). Experimental validation was then performed using Omnimagnets[19], which are designed to serve as approximate dipole-field sources, each comprising three co-located and mutually orthogonal electromagnets. A copper sphere floated in a raft in a container of water above four Omnimagnets (see Fig. 3e and Supplementary Information 7), serving as an Earth-based microgravity simulator with 3-DOF mobility in a horizontal plane. We performed 2-DOF position control, with and without 1-DOF orientation control (see Fig. 3f, g).

With our proposed method, 6-DOF manipulation of conductive non-magnetic spheres is achievable. In contrast, 6-DOF manipulation of ferromagnetic objects is only possible for complex geometries[23], with 5-DOF typical of most simple geometries and only 3-DOF achievable for soft-magnetic spheres[1]. The forces and torques generated using the proposed method are likely to be orders of magnitude smaller than those generated using ferromagnetism with comparable parameters, as indicated by the relatively slow manipulation demonstrations of Fig. 3, but they enable manipulation of objects that ferromagnetic methods do not (further discussion in Supplementary Information 8).

Manipulation with six DOF of ferromagnetic objects can be accomplished using eight static electromagnets[24,25], or eight permanent magnets at fixed positions with each having the ability to rotate about an axis orthogonal to its dipole axis[26]. Our numerical simulations showed that six rotating-dipole sources is sufficient for 6-DOF manipulation of conductive spheres; however, this number should not be assumed to be necessary. Since all wrenches have a repulsive force component, when manipulating an unconstrained object, the sources must surround the object to some degree. Analysing the manipulability of different numbers and arrangements of sources is left as an open problem.

In terms of modelling, thus far we have only considered solid spheres. A natural next step would be to consider hollow spheres and other simple geometric objects (such as cuboids or cylinders), which is likely to require more complicated models. It is unclear whether the best approach will be to explicitly model these objects or whether the sphere model can be used in conjunction with learning-based approaches for control. Although we have shown that a simplified approach using canonical positions and actuating one dipole-field source at a time is sufficient to perform dexterous manipulation,
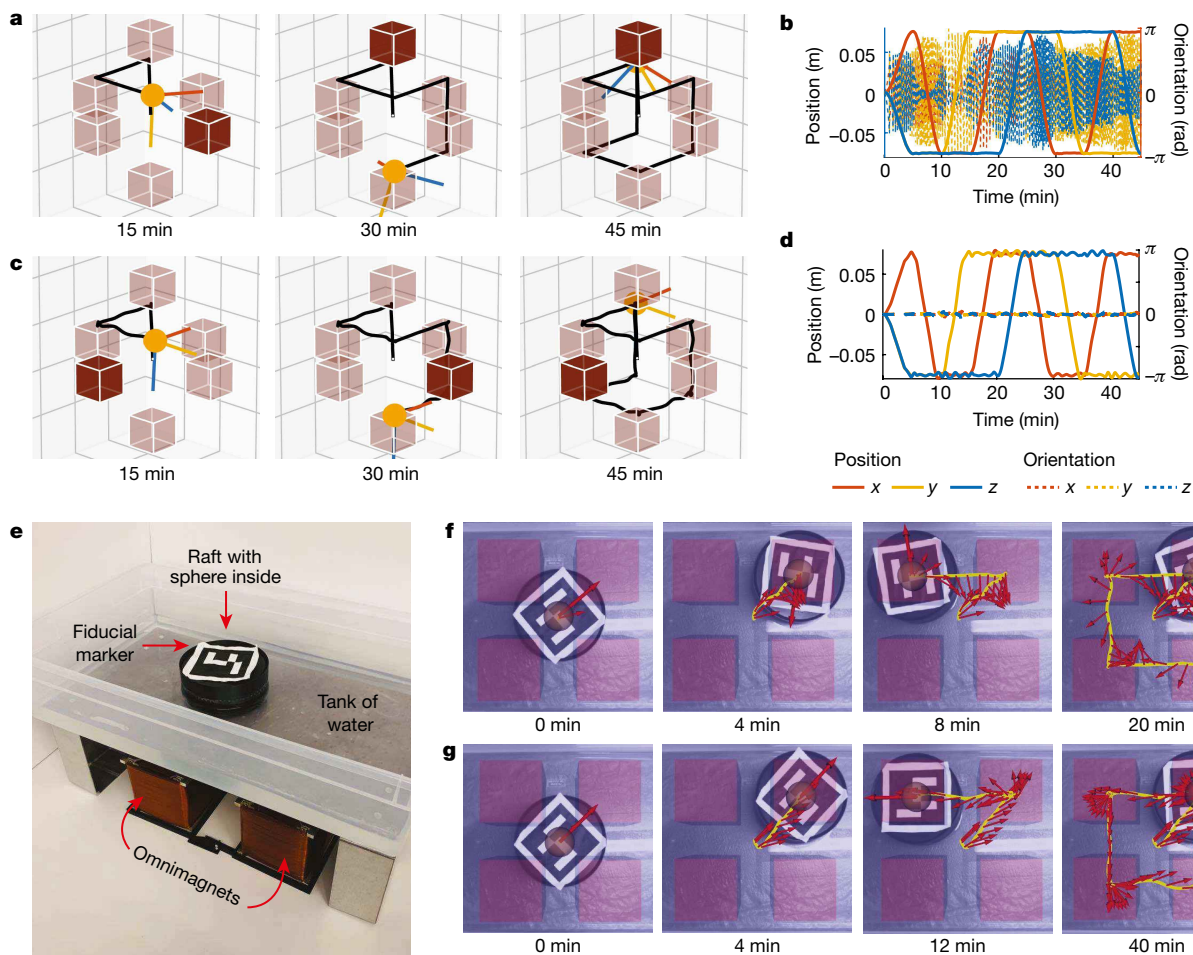
Fig. 3 | Dexterous manipulation of a copper sphere in simulated microgravity. See Supplementary Videos 1–4. **a**, **b**, Numerical simulation with 3-DOF position control along the edges of a cube (the black line is the path taken) and uncontrolled orientation using six dipole field sources (brown cubes, with the highlighted cube indicating the active source at the given instant; **a**), with the resulting 6-DOF pose (**b**). **c**, **d**, Numerical simulation with 6-DOF position and constant-orientation control (**c**), with the resulting 6-DOF pose (**d**). **e**, Experimental set-up with a copper sphere in a raft on water over four Omnimagnets. **f**, Experiments with 2-DOF position control along the edges of a square and uncontrolled orientation (the yellow line is the path taken, and red arrows depict the orientation). **g**, Experiments with 2-DOF position control and 1-DOF orientation control, with sharp turns at the corners.

it is probably suboptimal. A general wrench model for arbitrary sphere positions relative to the rotating dipole, and understanding the nonlinear nature of superposition, are both left as open problems.

Online content

Any methods, additional references, Nature Research reporting summaries, source data, extended data, supplementary information, acknowledgements, peer review information; details of author contributions and competing interests; and statements of data and code availability are available at https://doi.org/10.1038/s41586-021-03966-6.

1. Abbott, J. J., Diller, E. & Petruska, A. J. Magnetic methods in robotics. *Annu. Rev. Control Robot. Auton. Syst.* **3**, 57–90 (2020).
2. Hertz, H. *Miscellaneous Papers* Chapter 2 [transl. Jones, D. E. & Schott, G. A.] (Macmillan, 1896).
3. Griffiths, D. J. *Introduction to Electrodynamics* 4th edition (Cambridge Univ. Press, 2017).
4. Nagel, J. R. Induced eddy currents in simple conductive geometries: mathematical formalism describes the excitation of electrical eddy currents in a time-varying magnetic field. *IEEE Antennas Propag. Mag.* **3**, 81–88 (2018).
5. Youngquist, R. C., Nurge, M. A., Starr, S. O., Leve, F. A. & Peck, M. A. A slowly rotating hollow sphere in a magnetic field: first steps to de-spin a space object. *Am. J. Phys.* **84**, 181–191 (2016).
6. Nurge, M. A., Youngquist, R. C. & Starr, S. O. A thick-walled sphere rotating in a uniform magnetic field: the next step to de-spin a space object. *Am. J. Phys.* **85**, 596–610 (2017).
7. Nurge, M. A., Youngquist, R. C. & Starr, S. O. Drag and lift forces between a rotating conductive sphere and a cylinderical magnet. *Am. J. Phys.* **86**, 443–452 (2018).
8. Sharma, K. K. et al. Space debris reduction using eddy currents. In *2018 Atmospheric Flight Mechanics Conf.*, 3161 (American Institute of Aeronautics and Astronautics, 2018).
9. Reinhardt, B. Z. & Peck, M. A. New electromagnetic actuator for on-orbit inspection. *J. Spacecraft Rockets* **53**, 241–248 (2016).
10. Liu, X., Lu, Y., Zhou, Y. & Yin, Y. Prospects of using a permanent mangetic end effector to despin and detumble an uncooperative target. *Adv. Space Res.* **61**, 2147–2158 (2018).
11. Smith, Y. R., Nagel, J. R. & Rajamani, R. K. Eddy current seperation for recovery of non-ferrous metallic particles: a comprehensive review. *Miner. Eng.* **133**, 149–159 (2019).
12. Buckingham, E. On physically similar systems; illustrations of the use of dimensional equations. *Phys. Rev.* **4**, 345 (1914).
13. Shan, M., Guo, J. & Gill, E. Review and comparison of active space debris capturing and removal methods. *Prog. Aerosp. Sci.* **80**, 18–32 (2016).
14. Mark, C. P. & Kamath, S. Review of active space debris removal methods. *Space Policy* **47**, 194–206 (2019).
15. Kessler, D. J., Johnson, N. L., Liou J. C. & Matney, M. The Kessler syndrome: implications to future space operations. *Adv. Astronaut. Sci.* **137**, AAS 10-016 (2010).
16. Opiela, J. N. A study of the material density distribution of space debris. *Adv. Space Res.* **43**, 1058–1064 (2009).
17. Pelrine, R. et al. Diamagnetically levitated robots: an approach to massively parallel robotic systems with unusual motion properties. *IEEE Int. Conf. Robotics and Automation*, 739–744 (2012).
18. Mirica, K. A., Ilievski, F., Ellerbee, A. K., Shevkoplyas, S. S. & Whitesides, G. M. Using magnetic levitation for three dimensional self-assembly. *Adv. Mater.* **23**, 4134–4140 (2011).

19. Petruska, A. J. & Abbott, J. J. Omnimagnet: an omnidirectional electromagnet for controlled dipole-field generation. *IEEE Trans. Magn.* **50**, 8400410 (2014).
20. Wright, S. E., Mahoney, A. W., Popek, K. M. & Abbott, J. J. The spherical-actuator-magnet manipulator: a permanent-magnet robotic end-effector. *IEEE Trans. Robot.* **33**, 1013–2924 (2017).
21. Petruska, A. J. & Abbott, J. J. Optimal permanent-magnet geometries for dipole field approximation. *IEEE Trans. Magn.* **49**, 811–819 (2013).
22. Lynch, K. M. & Park, F. C. *Modern Robotics: Mechanics, Planning, and Control* (Cambridge Univ. Press, 2017).
23. Diller, E., Giltinan, J., Lum, G. Z., Ye, Z. & Sitti, M. Six-degree-of-freedom magnetic actuation for wireless microrobotics. *Int. J. Robot. Res.* **35**, 114–128 (2016).
24. Kummer, M. P. et al. OctoMag: an electromagnetic system for 5-DOF wireless micromanipulation. *IEEE Trans. Robot.* **26**, 1006–1017 (2010).
25. Petruska, A. J. & Nelson, B. J. Minimum bounds on the number of electromagnets required for remote magnetic manipulation. *IEEE Trans. Robot.* **31**, 714–722 (2015).
26. Ryan, P. & Diller, E. Magnetic actuation for full dexterity microrobotic control using rotating permanent magnets. *IEEE Trans. Robot.* **33**, 1398–1409 (2017).

Article

Competing interests J.J.A. has patents and patents pending on electromagnet and permanent-magnet devices designed to generate rotating magnetic dipole fields. The other authors declare no competing interests.

Additional information

Supplementary information The online version contains supplementary material available at https://doi.org/10.1038/s41586-021-03966-6.
Correspondence and requests for materials should be addressed to Jake J. Abbott.
Peer review information *Nature* thanks Eric Diller and the other, anonymous, reviewer(s) for their contribution to the peer review of this work.
Reprints and permissions information is available at http://www.nature.com/reprints.